# SPECTRAL CHARACTERISTICS ANALYSIS AND EXTRACTION OF MICRO-PATCHES BASED ON THE HYPERSPECTRAL DESERT STEPPE IMAGES

/

# 基于高光谱荒漠草原的微斑块光谱特征分析与提取

**Xinchao GAO[1)], Jianmin DU*[1)], Yuge BI[1)], Weiqiang PI[2)], Xiangbing ZHU[1)], Yanbin ZHANG[1)]**

[1)] Inner Mongolia Agricultural University, College of Mechanical and Electrical Engineering, Inner Mongolia, China

[2)] School of Mechanical and Electrical Engineering and Automotive Engineering, Huzhou Vocational and Technical College, Huzhou / China

*Tel:+86-0471-4309215; E-mail: xinchao0616@163.com*

*DOI: https://doi.org/10.35633/inmateh-67-12*

***Keywords:*** *Image processing; Desert grassland; Hyperspectral image; Microplaques; MSA; Threshold division*

## ABSTRACT

*In hyperspectral remote sensing images, desert steppe vegetation, bare soil, and rat holes appear as micro-patches. The spectral feature analysis of micro-patches is the basis for identification and classification and also the basis for quantitative remote sensing monitoring of ground objects. Taking the micro-patches of desert steppe in Inner Mongolia as the research object, the spectral reflectance of different micro-patches was extracted, and a variety of vegetation indices were calculated respectively. The spectral characteristics of different micro-patches were quantitatively analyzed, and the micro-patches spectral analysis method was proposed to realize the classification of high-resolution hyperspectral images of surface micro-plaques of desert steppe. The results showed that: (1) There are pronounced differences in the spectral reflectance of the three types of surface micro-patches. The vegetation has apparent characteristics in the green wave reflection peak and the red wave absorption valley. The spectral reflectance of the bare soil is higher than that of the mouse hole, and the two have been increasing. The trend is increasing slowly; (2) The proposal and application of the MSA(micro-patch spectral analysis) index can effectively realize the identification and classification of surface micropatches, and the Kappa coefficient has reached 0.906 through confusion matrix verification. The above spectral analysis method realizes the classification and identification of complex ground objects using near-ground remote sensing images. It provides new ideas and methods for accurate quantitative statistics of desert grassland ecological information.*

## 摘要

*高光谱遥感图像中荒漠草原植被、裸土、鼠洞均表现为微斑块，对微斑块进行光谱特征分析是识别分类的基础，同时也是定量遥感监测地物的基础。以内蒙古荒漠草原微斑块为研究对象，提取不同微斑块的光谱反射率，分别进行多种植被指数运算，定量分析不同微斑块的光谱特征，并提出微斑块光谱分析法，实现了对采集的高分辨率的荒漠草原地表微斑块高光谱图像分类研究。结果表明：（1）三类地表微斑块光谱反射率存在明显差异，植被在绿波反射峰与红波吸收谷表现特征明显，裸土的光谱反射率高于鼠洞且二者一直呈上升趋势缓慢增长；（2）MSA 指数的提出与应用有效地实现了地表微斑块的识别与分类，经混淆矩阵验证 Kappa 系数达到 0.906。上述光谱分析方法实现了利用近地面遥感图像对复杂地物的分类与识别，为荒漠草原生态信息的精确量化统计提供了新的思路与手段。*

## INTRODUCTION

The grassland ecosystem is continuously degraded by natural and human factors, manifested as low vegetation community, reduced population number, severe loss of soil organic matter, and apparent salinization trend *(Lyu et al, 2020, Wang et al, 2020)*. The traditional monitoring of grassland degradation through artificial field investigation, the proportion of degraded indicator grass species in the sample and the hole coefficient in the area, were calculated. The grassland degradation grade was evaluated according to the grassland degradation standard, and the statistical cycle was time-consuming and laborious. With the development of science and technology, satellite remote sensing is widely used in the ground investigation *(Sun et al, 2019)*. *Donovan, (2021),* obtained hyperspectral images from the EO-1 Hyperion satellite and realized the detection of different degrees of forest leaves based on the vegetation index. Based on Sentinel-1, Sentinel-2 satellite data, and digital soil images, the relationship between soil fertilizer and irrigated wheat yield in Nepal was obtained, and an accurate soil nutrient management plan was proposed *(Campolo et al, 2021)*.

*Tomáš Bucha, (2021),* used radar and optical multi-temporal data to establish a comprehensive prediction model through multiple regression and realized the aboveground biomass estimation of abandoned agricultural land in the Western Carpathians. Based on satellite remote sensing image of aboveground biomass ( AGB ), the distribution map of grazing intensity ( ungrazed, light grazed, moderate grazed and heavy grazed ) in Xilinguole grassland was drawn by multi-spectral reflectance simulation (*Li et al, 2016*). *Laiskhanov, (2021)* compiled a map of landscape drying and soil salinization by comparing the satellite data of the Ili River delta in 1979 and 2019. In summary, satellite remote sensing has realized the coverage and biomass calculation of typical grassland vegetation and agricultural land, but studies based on desert grassland are rarely reported.

With the acceleration of grassland ecosystem degradation, higher requirements have been put forward for high-precision and real-time dynamic monitoring of grassland degradation *(Yan et al, 2019).* The existing vegetation index cannot realize the fine division of the surface micropatches of the desert steppe. The spatial resolution of satellite remote sensing data is low. At the same time, due to its hardware limitations and the complex background environment in the data collection process, “the same thing with different spectrums, different things with the same spectrum” appears between different micropatches, which leads to identifying confusion during classification. Hyperspectral micropatch sensing data has the advantages of the high temporal-spatial resolution, multi-band, and a large amount of information *(Zhu et al, 2021, Guo et al, 2018)*. In this study, the hyperspectral data of desert grassland micro-patches were used to analyze the spectral characteristics, calculate various vegetation indices, analyze the spectral differences between different micro-patches, and finally construct the MSA identification and classification model, which is used for the identification and classification of hyperspectral remote sensing systems in desert grasslands. It provides a basis for statistics, and a new solution for monitoring grassland degradation.

## MATERIALS AND METHODS

### Overview of experimental area

The experiment was carried out in Gegentala Grassland (41.78°N, 111.88°E) in Siziwang Banner, Inner Mongolia Autonomous Region. The region is located in Eurasia and belongs to a semi-dry-mid temperate monsoon climate. It has high temperature and little rain in summer, cold and dry in winter, low annual average precipitation, and extensive evaporation. The unique climatic characteristics and geographical location decrease the overall vegetation coverage from southeast to northwest, and the vegetation coverage rate is low, with the typical geographical representation of a desert steppe *(Gao et al, 2020).*

In the experiment, 50 quadrats with a size of 50 cm × 50 cm including rat holes, were randomly placed in a grazing area of 3 $km^2$. To reduce external interference and ensure vertical sunlight, the collection time was set from 11:00 to 13:00. The hyperspectral data is recorded in the hyperspectral imager controller. The hyperspectral data contains 256 bands, the spectral range covers 400 nm~1000 nm, and the spectral resolution is 3.5 nm. The hyperspectral image is shown in the figure 1.

**Fig. 1 - Hyperspectral raw data**

### Micropatch region of interest selection

The micropatches in desert steppe are nested and interlaced. Three types of micropatches were selected for analysis in this study. According to their distribution characteristics and the area proportions of various kinds of micropatches in the region, the regions of interest of micropatches were determined according to visual interpretation (Table 1).

Table 1

**Pixel information contained in the ROI of each micropatch**

| Microplaque Type | Number of pixels | Polygon features | Point features |
|---|---|---|---|
| **Vegetation** | 3392 | 6/3196 | 196 |
| **Bare soil** | 2056 | 5/1823 | 233 |
| **Rat hole** | 752 | 1/752 | 0 |

**Micropatch reflectance curve characteristics**

The spectral reflectance curve characteristics of the three types of micropatches are different (Figure 2). The background of the rat hole is relatively simple, it appears black under sunlight, and the reflectance to light is low on the whole waveband, always lower than 0.05. The reflectivity of visible light in the bare soil increases proportionally, and the overall performance is higher than that of the mouse hole. The spectral reflectance of vegetation is slightly higher than that of bare soil. At 450 nm~560 nm, vegetation is affected by its high chlorophyll content, and the reflectance is higher than that of bare soil, thus forming a prominent reflection peak; while at 560 nm~700 nm, the reflectance of vegetation is slightly lower than that of bare soil; in the red light region and near-infrared region after 700 nm, the reflectance of vegetation rises sharply and then tends to be flat. In this region, the reflectance of vegetation reaches about 0.45, and that of bare soil reaches 0.25.

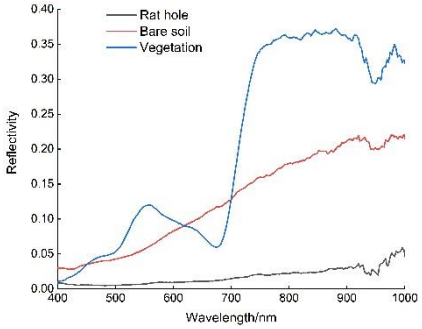


**Fig. 2 - Spectral reflectance curve of each micropatch**

Considering that the spectral reflectance jitter of micro-patches in the near-infrared region is relatively apparent, to highlight further the spectral characteristics of the three types of micro-patches, the first-order derivative calculation is performed on the spectra in the full-band range (Figure 3), and the formula is as follows:

$$\rho'_{\lambda_i} = \frac{\left(\rho_{\lambda_{i+1}} - \rho_{\lambda_{i-1}}\right)}{2\Delta\lambda} \quad (1)$$

Where: $\rho'_{\lambda_i}$ represent the first derivative value at band $\lambda_i$, $\rho_{\lambda_{i+1}}$ represents the spectral reflectance at $\lambda_{i+1}$, $\rho_{\lambda_{i-1}}$ represents the spectral reflectance at $\lambda_{i-1}$, and $\Delta\lambda$ represents the number difference of bands.

The results show that only the vegetation has the prominent ρ red edge, yellow edge, and blue edge characteristics; the red edge is located at 711.2 nm, the slope is 0.02348; the yellow edge is located at 562.3 nm, the slope is -0.00281; the blue edge is located at 510.9 nm, the slope is 0.004837. The second is that the blue edge of the bare earth is located at 515.5 nm, and the slope is 0.002454. The first-order spectral reflectance of the rat hole is still flat in the visible light range without fluctuation.

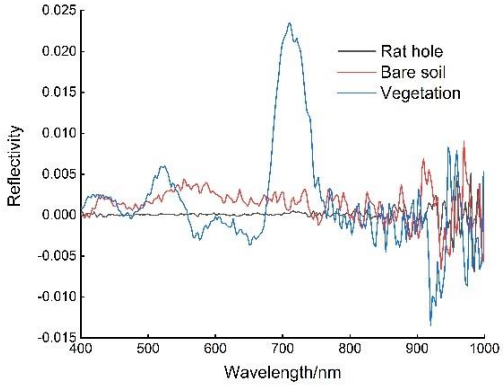


**Fig. 3 - The first derivative curve of the spectral reflectance of each micro-patch**

**Micropatch vegetation index calculation**

To further analyze the spectral characteristics of micro-patches, the normalized vegetation index (NDVI), ratio vegetation index (RVI), soil-adjusted vegetation index (SAVI), and enhanced vegetation index (EVI) were calculated according to the distribution characteristics of surface micro-patches in a typical desert steppe. NDVI, RVI, and EVI can better divide vegetation and non-vegetation but cannot accurately separate non-vegetation; SAVI can distinguish between rat holes and bare soil but cannot realize the division of vegetation and non-vegetation. The results show that there is vegetation. There is still a specific deviation in the recognition and classification accuracy of the index *(Zhang et al, 2020)*.

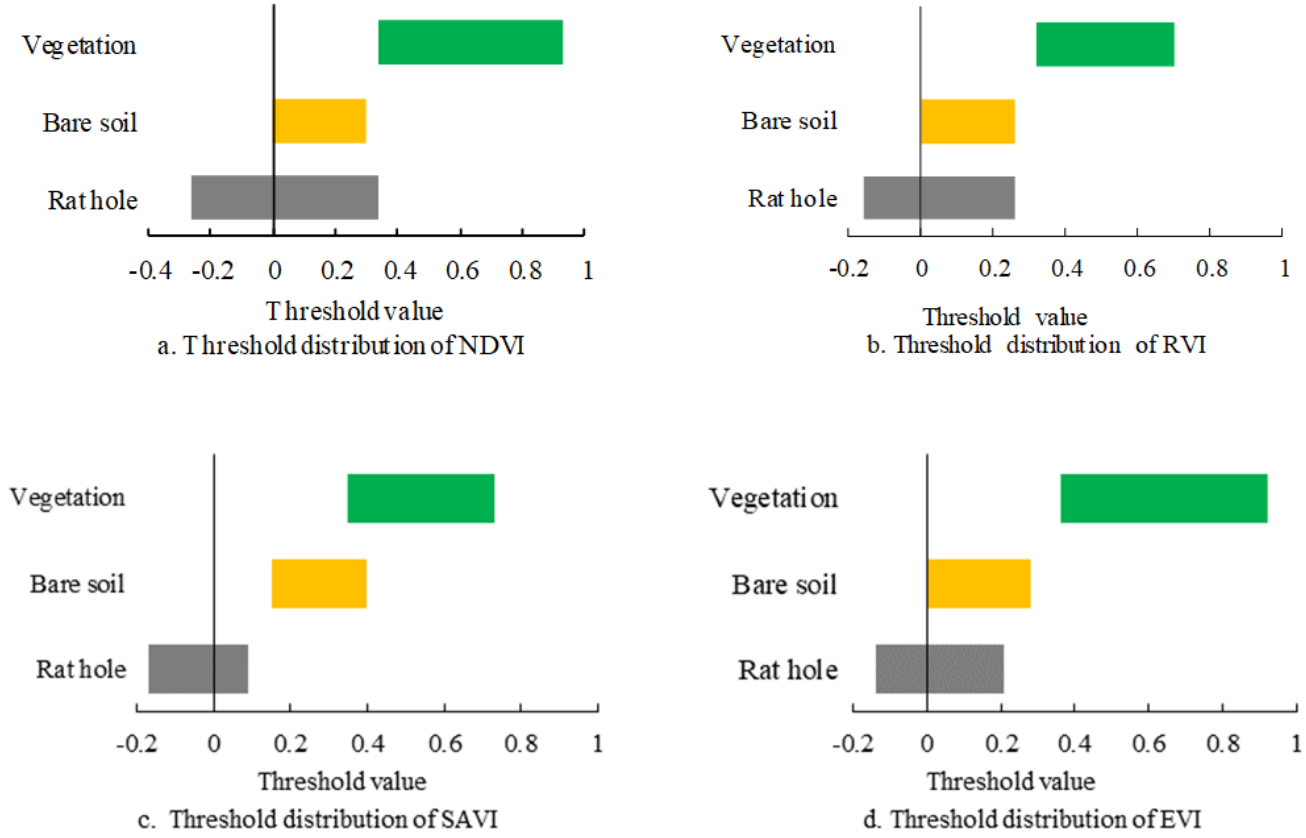


**Fig. 4 - Threshold distribution of different vegetation indices**

## PROPOSAL FOR MSA INDEX

Conventional index methods such as NDVI can only achieve the extraction of a single ground object. There is a severe overlap between the distribution areas of different micro-patches, which cannot meet the classification requirements of surface micro-patches in a desert steppe. Therefore, the MSA index is proposed to achieve the fine division of micro-patches.

**Data preprocessing**

External factors such as clouds and light easily disturb the data collection process. It is necessary to remove the hyperspectral images with uneven exposure and then correct the reflectivity of the standard spectral images to eliminate the radiation errors caused by external interference to the hyperspectral images, to obtain a standard reflectance spectrum.

Affected by various factors such as Gaussian noise, stripe noise, and external environment in the process of hyperspectral data acquisition, the reflectivity curve of each pixel is relatively chaotic, which leads to the loss of a lot of information in the hyperspectral image, reduces the application accuracy of hyperspectral images in ground object classification and target pixel detection *(Zeng et al, 2019)*. The existence of noise has caused significant fluctuations in the spectral data, resulting in a significant deviation of the actual spectral reflectance, which is very unfavorable for the research of ground object classification. Therefore, it is necessary to perform mathematical operations on the hyperspectral image's entire waveband to eliminate the interference of the subsequent ground object classification processing.

The smooth noise reduction formula is as follows:

$$\rho = \text{smooth}(s1, 5) \tag{2}$$

Where: ρ represents the spectral curve after processing, s1 represents the spectral curve, and 5 represents the weighted coefficient of smooth noise reduction.

**Proposal for MSA Index**

The spectral curves of 50 pure pixels of three types of micro-patches in the region of interest are respectively selected for mean calculation, and the standard spectral curves of the pure pixels are extracted. The formula is as follows:

$$Average\_Ref = \frac{\sum_{i=1}^{n} b_i}{n} \tag{3}$$

Where: $b_i$ is the selected band's reflectivity and $Average\_Ref$ is the average reflectivity, $n$ is taken as 50.

Analysis of the standard spectral curve of the micro-patches (Figure 5) found that the vegetation spectral curve showed a slow upward trend in the range of 400 nm~560 nm blue-green light, forming the first reflection peak. Due to the high chlorophyll content in the desert steppe vegetation, the carotenoid content is relatively low. The absorption is strong in the near-red light band range of 560 nm~680 nm, and the reflectivity shows a downward trend. Then in the red light and near-infrared band, the reflectance shows a stronger upward trend, and the peak value of the reflectance is close to 0.5. Bare soil and rat holes do not have this prominent feature. The rising trend of bare soil in the illumination range of 400 nm~560 nm was similar to that of vegetation, and the spectral reflectance increased with the increase of wavelength. The rat hole is flat in the whole range, and there is no apparent growth trend. The reflectivity of the three types of micropatches tends to be balanced in the near-infrared band. In summary, based on the above differences in spectral characteristics, a surface micropatch spectral analysis index ($MSA$) model is established, and the formula is as follows:

$$MSA = \frac{(\rho_{NIR} - \rho_R)}{10(\rho_R - \rho_G)} \tag{4}$$

Where $MSA$ is the micropatch index, $\rho_G$ is the green band, $\rho_{NIR}$ in the near-infrared band, and $\rho_R$ is the red band.

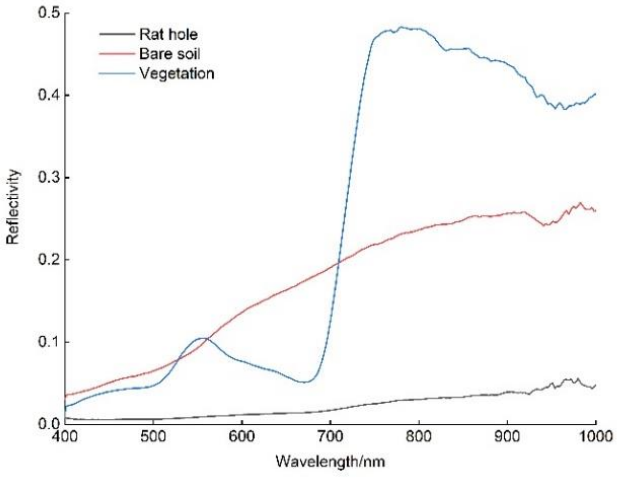


**Fig. 5 - The mean curve of spectral reflectance of each micropatch after denoising**

## RESULTS AND DISCUSSION

**Classification result**

The MSA index calculation was performed on five micro-patch samples, including mouse holes. To reduce the influence of errors caused by the band calculation, this study selected 20 wavelength bands of green light, red light, and near-infrared, respectively, for calculation. After the operation, according to the distribution of micro-patches in the random quadrat, the proportions of pixels are selected as 5%, 10%, 30%, 50%, 70%, and 90% as the threshold boundary nodes for threshold statistics (Table 2).

Table 2

**Threshold statistics of MSA index**

| Data number | The different pixel threshold percentage | | | | | |
|---|---|---|---|---|---|---|
| | 5% | 10% | 30% | 50% | 70% | 90% |
| R1 | 0.09265 | 0.09984 | 0.11465 | 0.12467 | 0.12678 | 0.14587 |
| R2 | 0.09386 | 0.10328 | 0.11527 | 0.12329 | 0.13583 | 0.14295 |
| R3 | 0.09785 | 0.10870 | 0.11677 | 0.12496 | 0.13665 | 0.15833 |
| R4 | 0.09931 | 0.10992 | 0.11760 | 0.12694 | 0.14376 | 0.14982 |
| R5 | 0.09523 | 0.11351 | 0.11782 | 0.13324 | 0.13292 | 0.13424 |
| B1 | 0.01428 | 0.02398 | 0.04876 | 0.05831 | 0.07651 | 0.08823 |
| B2 | 0.01593 | 0.03356 | 0.04589 | 0.05913 | 0.07791 | 0.08941 |
| B3 | 0.02975 | 0.03587 | 0.04671 | 0.05992 | 0.07998 | 0.09230 |
| B4 | 0.02769 | 0.04981 | 0.03587 | 0.06134 | 0.07821 | 0.08769 |
| B5 | 0.02876 | 0.04127 | 0.05912 | 0.06325 | 0.07993 | 0.09184 |
| V1 | -0.23765 | -0.23687 | -0.47198 | -0.56713 | -0.69341 | -0.78491 |
| V2 | -0.13721 | -0.41874 | -0.45980 | -0.59173 | -0.68274 | -0.71463 |
| V3 | -0.27931 | -0.33791 | -0.51381 | -0.55791 | -0.66419 | -0.86391 |
| V4 | -0.15920 | -0.45217 | -0.45917 | -0.61598 | -0.77529 | -0.81429 |
| V5 | -0.17094 | -0.36791 | -0.46098 | -0.66790 | -0.71451 | -0.86109 |

The results show that the minimum CV value (Cursor Value) of various samples is -0.86391, the maximum value is 0.15833, and the CV value distribution of ground objects is relatively continuous and uniform. To avoid random error interference, [-1, 0.2] is used as the threshold range for MSA to calculate micro-patches.

After the MSA operation, the micro-patches are all represented as single-band grayscale images (Figure 6). The corresponding CV values of each pixel are different. As the CV value of the pixel decreases, the color becomes brighter, and the vegetation color is the most brilliant. In this study, based on the visual interpretation method, the CV value statistics were compared with the positions of different micropatches in the original image to determine the threshold range of three types of micro-patches (Figure 7). The vegetation threshold range is [-0.86391, 0], the bare soil threshold range is [0, 0.09264]. The mouse hole threshold range is [0.09264, 0.15833].

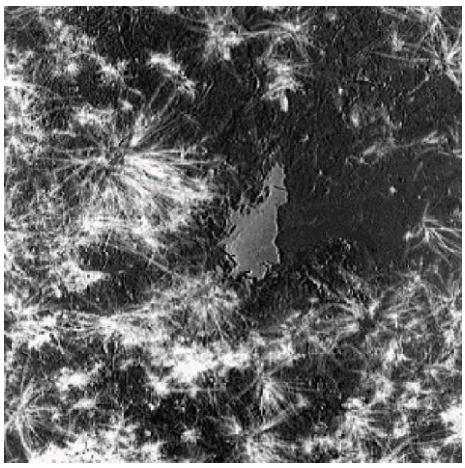

**Fig. 6 - Grayscale image of MSA operation**

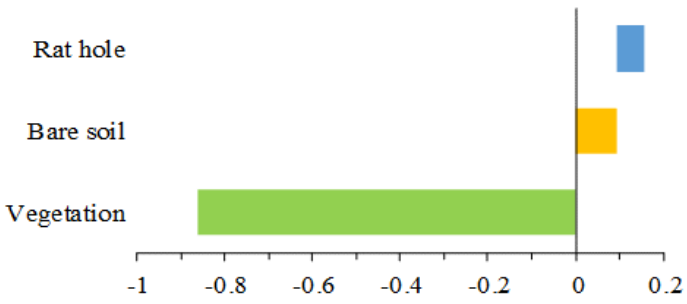


**Fig. 7 - Threshold distribution between micropatches**

To avoid the threshold division's contingency and verify the threshold interval's robustness, this study again selects different samples to perform the MSA index operation. After the operation, the results are divided according to the threshold value (Figure 8).

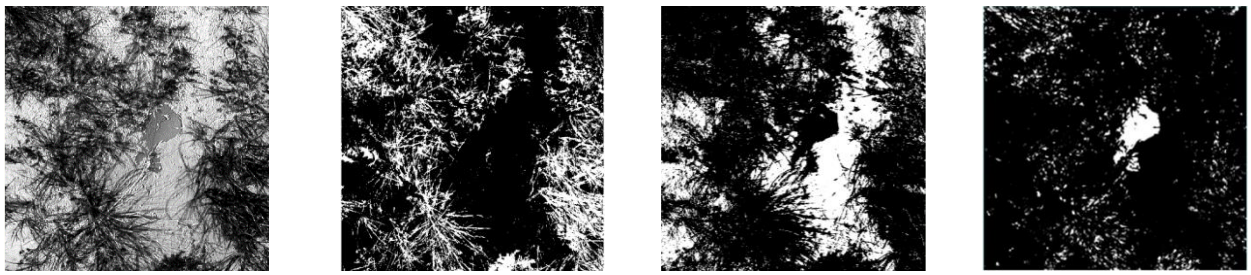

a. MSA operation grayscale image b. vegetation c. bare soil d. rat hole

**Fig. 8 - Comparison of the positions of each micro-plaque**

**Accuracy verification**

The Kappa coefficient is calculated based on the confusion matrix and used to measure the accuracy of surface classification in the remote sensing field *(Pan et al, 2017)*. The formula is as follows:

$$K = \frac{N\sum_{i=1}^{n} x_{ii} - \sum_{i=1}^{n} x_{i+}x_{+i}}{N^2 - \sum_{i=1}^{n} x_{i+}x_{+i}} \quad (5)$$

where: $K$ represents the Kappa coefficient, $x_{ii}$ represents the mixing matrix, $n$ represents rows and columns, $x_{i+}$ represents the sum of the error matrix in the $i$ row, $x_{+i}$ represents the sum of the error matrix in the $i$ column, and $N$ represents the sum of the number of pixels in the image.

After data preprocessing, the remaining quadrats are subjected to accuracy verification, and the data images obtained after the MSA index operation are subjected to the best separability threshold verification. The obtained mask file is subjected to pixel data statistics, the confusion matrix is listed (Table 3), the calculated Kappa coefficient is 0.906, and the overall classification accuracy is 92.1%. The results show that the MSA index method has a better effect on identifying and classifying desert steppe micropatches.

**Table 3**

**MSA-based confusion matrix**

| MSA | Classification result | | | |
|---|---|---|---|---|
| | Bare soil | Vegetation | Rat hole | Total |
| **Bare soil** | 1908 | 124 | 63 | 2095 |
| **Vegetation** | 96 | 3174 | 58 | 3328 |
| **Rat hole** | 52 | 94 | 631 | 777 |
| **Total** | 2056 | 3392 | 752 | 6200 |

**Result analysis**

After the image classification results (Figure 8) and the accuracy verification (Table 4), it was found that the MSA index has good applicability for the classification of desert steppe micropatches, and the classification accuracy is high. However, after analysis, it is found that there are still errors in the classification process of various pixels. Mainly due to the staggered distribution of various micro-patches and the change of the angle of direct sunlight during the data collection process, some pixels are blended during the data collection process, and the difference in spectral reflectance of characteristic bands is weakened, resulting in misclassification. Compared with the mask and original image pixels, the misclassified mixed pixels are mainly located at the edge of the mouse hole, the shadow area under direct sunlight, and the intersection position of micro-plaques. Based on this error, higher requirements are put forward for the micro-patches division.

Table 4

**Kappa coefficient and overall classification accuracy**

| Accuracy category | coefficient |
|---|---|
| **Kappa coefficient** | 0.906 |
| **Overall classification accuracy** | 92.1% |

## CONCLUSIONS

Desert steppe has low plants, narrow leaves, and random distribution among different ground objects, which leads to difficulty in classification. In response to the above problems, this study first proposed and applied the MSA method to realize the identification of micro-patches on the surface of desert grasslands, breaking through the limitations of traditional methods and providing a theoretical basis for the use of remote sensing methods to calculate the coverage of grassland vegetation.

The main conclusions are as follows:

1) Through the analysis of the spectral characteristic curve of the micro-patches in the area of interest, and based on the first-order operation of the spectral reflectance curve, three types of micro-patches with relatively large spectral characteristics were found;

2) For the desert steppe NDVI, SAVI, RVI, EVI operations were performed on micropatches, and after comparing their classification effects, it was found that the four types of indices could not achieve fine classification for the three types of micropatches, and there was an intersection between different micropatch thresholds;

3) MSA method It can weaken the influence of noise on hyperspectral images, restore the actual spectral characteristics of surface micro-patches, break the traditional methods of difficult statistics and high risk coefficients of desert grassland features, and improve the classification accuracy;

4) From the verification results looking at the MSA method not only improves the classification accuracy of grassland surface micropatch processing, but also effectively simplifies the hyperspectral classification process.

The MSA provides a data analysis method for the vegetation inversion of desert grasslands. It can be widely used in classifying surface micropatches in the grassland degradation process to achieve the grassland monitoring effect. This is crucial to identifying and classifying surface micropatches in a desert steppe. Problems in the data classification process include misclassification of mixed pixels and differences in reflectivity of similar micro-patches. These problems lead to specific errors in classification accuracy. Therefore, it is still necessary to strengthen the fine classification of surface micro-patches to improve the classification accuracy. In the following experiment, the above method will be applied to UAV low altitude hyperspectral data analysis to achieve rapid, large area and accurate identification and classification of desert grassland surface micro patches and provide the possibility for extensive area grassland degradation monitoring in the future.

## ACKNOWLEDGEMENT

This project was funded by the National Natural Science Foundation of China (NSFC) (31660137) and the Scientific Research Project of Inner Mongolia Autonomous Region (NJZY21518).

## REFERENCES

[1] Bucha T., Papčo J., Sačkov I., Pajtík J., Sedliak M., Barka I., Feranec J. (2021). Woody Above-Ground Biomass Estimation on Abandoned Agriculture Land Using Sentinel-1 and Sentinel-2 Data [J]. *Remote Sensing*, 13(13):2488.

[2] Campolo J., Güerea D., Maharjan S., et al. (2021). Evaluation of soil-dependent crop yield outcomes in Nepal using ground and satellite-based approaches [J]. *Field Crops Research*, 260(4):107987.

[3] Gao Y.N., Wang H.L., Zhao M.L. (2020) Spatio-temporal dynamics of vegetation net primary productivity and its response to climate change in desert steppe, Inner Mongolia: A case study in Siziwang Banner (内蒙古荒漠草原植被 NPP 时空变化及气候因子分析：以四子王旗为例) [J]. *Journal of China Agricultural University*, 25(08):100-107.

[4] Guo Y.B., Zhuo L., Tao H.Y., Cao J.J., Wang Fang (2018). Spatial-Spectral Preprocessing based on Nonnegative Matrix Factorization to Unmix Hyperspectral Data (基于空谱初始化的非负矩阵光谱混合像元盲分解). *Remote Sensing Technology and Application*, 33(2): 216-226.

[5] Laiskhanov S.U., Poshanov M.N., Smanov Z M ,et al.( 2021) A Study of the Processes of Desertification at the Modern Delta of the Ili River with the Application of Remote Sensing Data[J]. *Journal of Ecological Engineering*, (3):169-178.

[6] Li F., Zheng J., Wang H., et al. ( 2016) Mapping grazing intensity using remote sensing in the Xilingol steppe region, Inner Mongolia, China[J]. *Remote sensing letters*, 7(4-6):328-337.

[7] Lyu X., Li X., Dang D. et al. (2017) A new method for grassland degradation monitoring by vegetation species composition using hyperspectral remote sensing [J]. *Ecological Indicators*, 2020, 114:106310.

[8] Pan H.T., Wang X., Wang X.T. (2017). Study on the effect of training samples on the accuracy of crop remote sensing classification (训练样本对农作物遥感分类的精度影响研究) [J]. *Infrared and Laser Engineering*, 46(S1): 143-150.

[9] Sun B., Li Z., Gao W. et al. (2019). Identification and assessment of the factors driving vegetation degradation/regeneration in drylands using synthetic high spatiotemporal remote sensing Data-A case study in Zhenglanqi, Inner Mongolia, China[J]. *Ecological indicators*, 107(12):105614.1-105614.16.

[10] Sdd A., Ml A., Yun Z.B. et al. (2020). Evaluating annual spruce budworm defoliation using change detection of vegetation indices calculated from satellite hyperspectral imagery [J]. *Remote Sensing of Environment*, 253.

[11] Wang J.F., He L., Lu S.J., Lü D., Huang T., Cao Q., Zang X.P., Liu B.Y. (2020). Photosynthetic vegetation cover response to precipitation on the Inner Mongolian Steppe（内蒙古不同类型草原光合植被覆盖度对降水变化的响应）[J]. *Acta Ecologica Sinica*, 40(16): 5620-5629.

[12] Yan J., Zhang G., Deng X. et al. (2019). Does Climate Change or Human Activity Lead to the Degradation in the Grassland Ecosystem in a Mountain-Basin System in an Arid Region of China? [J]. *Sustainability*, 11(9):2618.

[13] Zhu N., Wang H., Ning X.G. (2021). Advances in remote sensing monitoring of grassland degradation (草地退化遥感监测研究进展) [J]. *Science of Surveying and Mapping*, 46(05):66-76.

[14] Zhang X., Chen X., Tian M., Fan Y., Ma J., Xing D. (2020) An evaluation model for aboveground biomass based on hyperspectral data from field and TM8 in Khorchin grassland, China. *PLoS ONE* 15(2): e0223934.

[15] Zeng H.J., Jiang J.W., Zhao J.J. et al. (2019). $L_{1-2}$ spectral-spatial total variation regularized hyperspectral image denosing ($L_{1-2}$空谱全变差正则化下的高光谱图像去噪) [J]. *Acta Photonica Sinica,* 48(10):214-228.